NASA/TM–2009-215705

Compressibility Considerations for κ-ω Turbulence Models in Hypersonic Boundary Layer Applications

C. L. Rumsey
Langley Research Center, Hampton, Virginia

April 2009

NASA STI Program . . . in Profile

Since its founding, NASA has been dedicated to the advancement of aeronautics and space science. The NASA scientific and technical information (STI) program plays a key part in helping NASA maintain this important role.

The NASA STI program operates under the auspices of the Agency Chief Information Officer. It collects, organizes, provides for archiving, and disseminates NASA's STI. The NASA STI program provides access to the NASA Aeronautics and Space Database and its public interface, the NASA Technical Report Server, thus providing one of the largest collections of aeronautical and space science STI in the world. Results are published in both non-NASA channels and by NASA in the NASA STI Report Series, which includes the following report types:

- TECHNICAL PUBLICATION. Reports of completed research or a major significant phase of research that present the results of NASA programs and include extensive data or theoretical analysis. Includes compilations of significant scientific and technical data and information deemed to be of continuing reference value. NASA counterpart of peer-reviewed formal professional papers, but having less stringent limitations on manuscript length and extent of graphic presentations.

- TECHNICAL MEMORANDUM. Scientific and technical findings that are preliminary or of specialized interest, e.g., quick release reports, working papers, and bibliographies that contain minimal annotation. Does not contain extensive analysis.

- CONTRACTOR REPORT. Scientific and technical findings by NASA-sponsored contractors and grantees.

- CONFERENCE PUBLICATION. Collected papers from scientific and technical conferences, symposia, seminars, or other meetings sponsored or co-sponsored by NASA.

- SPECIAL PUBLICATION. Scientific, technical, or historical information from NASA programs, projects, and missions, often concerned with subjects having substantial public interest.

- TECHNICAL TRANSLATION. English-language translations of foreign scientific and technical material pertinent to NASA's mission.

Specialized services also include creating custom thesauri, building customized databases, and organizing and publishing research results.

For more information about the NASA STI program, see the following:

- Access the NASA STI program home page at *http://www.sti.nasa.gov*

- E-mail your question via the Internet to help@sti.nasa.gov

- Fax your question to the NASA STI Help Desk at 443-757-5803

- Phone the NASA STI Help Desk at 443-757-5802

- Write to:
  NASA STI Help Desk
  NASA Center for AeroSpace Information
  7115 Standard Drive
  Hanover, MD 21076-1320

NASA/TM–2009-215705

Compressibility Considerations for κ-ω Turbulence Models in Hypersonic Boundary Layer Applications

C. L. Rumsey
Langley Research Center, Hampton, Virginia

National Aeronautics and
Space Administration

Langley Research Center
Hampton, Virginia 23681-2199

April 2009

Available from:

NASA Center for AeroSpace Information
7115 Standard Drive
Hanover, MD 21076-1320
443-757-5802

Abstract

The ability of k-ω models to predict compressible turbulent skin friction in hypersonic boundary layers is investigated. Although uncorrected two-equation models can agree well with correlations for hot-wall cases, they tend to perform progressively worse - particularly for cold walls - as the Mach number is increased in the hypersonic regime. Simple algebraic models such as Baldwin-Lomax perform better compared to experiments and correlations in these circumstances. Many of the compressibility corrections described in the literature are summarized here. These include corrections that have only a small influence for k-ω models, or that apply only in specific circumstances. The most widely-used general corrections were designed for use with jet or mixing-layer free shear flows. A less well-known dilatation-dissipation correction intended for boundary layer flows is also tested, and is shown to agree reasonably well with the Baldwin-Lomax model at cold-wall conditions. It exhibits a less dramatic influence than the free shear type of correction. There is clearly a need for improved understanding and better overall physical modeling for turbulence models applied to hypersonic boundary layer flows.

1 Introduction

Compressibility is typically not considered to be important for wall-bounded turbulent flows over a wide range of Mach numbers. As stated in Wilcox [1] (p. 239): "Generally speaking, compressibility has a relatively small effect on turbulent eddies in wall-bounded flows. This appears to be true for Mach numbers up to about 5 (and perhaps as high as 8), provided the flow doesn't experience large pressure changes over a short distance such as we might have across a shock wave. At subsonic speeds, compressibility effects on eddies are usually unimportant for boundary layers provided $T_w/T_e < 6$."

The hypothesis of Morkovin [2] states that the compressibility effects on turbulence can be accounted for by mean density variations alone. For many applications, this hypothesis has proved correct in that good results can be obtained for mean velocity and temperature fields using incompressible turbulence models extended directly to compressible turbulent boundary layers. Furthermore, So et al. [3] have shown the Morkovin hypothesis to be equally applicable for prediction of the turbulence field itself, for flat plate boundary layers up to a Mach number of at least 10. They state: "there is indeed a dynamic similarity of the incompressible and compressible mean and turbulence field, and the Morkovin hypothesis is valid for both fields." In other words, for many subsonic through hypersonic boundary layer applications, the incompressible forms of turbulence models (with mean density variations accounted for) are expected to be reasonable approximations.

The most common classes of compressibility correction for Reynolds-averaged Navier-Stokes (RANS) turbulence models were developed for the purpose of improving correlations with experiment for free shear layer or jet spreading rates. See, e.g., Refs. 4–6. However, what we are concerned with here is primarily (attached) hypersonic boundary layer flow. In this paper, compressibility corrections (particularly applicable to boundary layer flows) from the literature are described. The focus here is solely on the k-ω form of two-equation models. The claim that compressibility corrections are not required for hypersonic boundary layer flows is investigated for a wide range of Mach numbers and wall-temperature boundary conditions.

The paper is organized as follows. First, several standard forms of the k-ω model are given. Then, compressibility corrections from the literature are described. Finally, results for hypersonic boundary layer flows are shown, and conclusions are made.

2 Standard Forms of Two-Equation Turbulence Models

2.1 Wilcox 1988

The original incompressible form of the Wilcox k-ω model [7], referred to here as Wilcox88, is written as:

$$\frac{Dk}{Dt} = \frac{\mathcal{P}}{\rho} - \beta^* \omega k + \frac{\partial}{\partial x_j}\left[(\nu + \sigma_k \nu_t)\frac{\partial k}{\partial x_j}\right] \tag{1}$$

$$\frac{D\omega}{Dt} = \frac{\gamma}{\mu_t}\mathcal{P} - \beta\omega^2 + \frac{\partial}{\partial x_j}\left[(\nu + \sigma_\omega \nu_t)\frac{\partial \omega}{\partial x_j}\right] \tag{2}$$

where $\nu = \mu/\rho$ and $\nu_t = \mu_t/\rho$. The eddy viscosity is given by:

$$\mu_t = \rho\frac{k}{\omega} \tag{3}$$

and the production term $\mathcal{P}$ is given by

$$\mathcal{P} = -\tau_{ij}\frac{\partial u_i}{\partial x_j} \tag{4}$$

where

$$\tau_{ij} = \rho\overline{u_i u_j} = -2\mu_t\left(S_{ij} - \frac{1}{3}\frac{\partial u_k}{\partial x_k}\delta_{ij}\right) + \frac{2}{3}\rho k\delta_{ij} \tag{5}$$

$$S_{ij} = \frac{1}{2}\left(\frac{\partial u_i}{\partial x_j} + \frac{\partial u_j}{\partial x_i}\right) \tag{6}$$

Note that the definition for τ_{ij} varies in the literature: sometimes it is defined with the opposite sign, and sometimes it is defined without the density. The definition does not matter as long as the production term is defined appropriately in Eq. (4), with $+2\mu_t S_{ij}(\partial u_i/\partial x_j)$ as the leading term in $\mathcal{P}$. In Eq. (5), the $-(1/3)(\partial u_k/\partial x_k)\delta_{ij}$ term and the $(2/3)\rho k\delta_{ij}$ term are often ignored for low-speed flows (the former term makes the strain rate tensor traceless in 3-D flows), but these both may be non-negligible for higher speed flows, or near stagnation regions. The constants are $\beta^* = 0.09$, $\sigma_k = 0.5$, $\gamma = 5/9$, $\beta = 3/40$, and $\sigma_\omega = 0.5$.

For clarity, the production term is expanded out here:

$$\mathcal{P} = 2\mu_t S_{ij}\frac{\partial u_i}{\partial x_j} - \frac{2}{3}\mu_t\left(\frac{\partial u_k}{\partial x_k}\right)^2 - \frac{2}{3}\rho k\frac{\partial u_k}{\partial x_k} \tag{7}$$

$$= \mu_t\left[\left(\frac{\partial u_i}{\partial x_j} + \frac{\partial u_j}{\partial x_i}\right)\frac{\partial u_i}{\partial x_j} - \frac{2}{3}\left(\frac{\partial u_k}{\partial x_k}\right)^2\right] - \frac{2}{3}\rho k\frac{\partial u_k}{\partial x_k} \tag{8}$$

Note that

$$S^2 \equiv 2S_{ij}S_{ij} = \frac{1}{2}\left(\frac{\partial u_i}{\partial x_j} + \frac{\partial u_j}{\partial x_i}\right)\left(\frac{\partial u_i}{\partial x_j} + \frac{\partial u_j}{\partial x_i}\right) = \left(\frac{\partial u_i}{\partial x_j} + \frac{\partial u_j}{\partial x_i}\right)\frac{\partial u_i}{\partial x_j} \tag{9}$$

So:

$$\mathcal{P} = \mu_t S^2 - \frac{2}{3}\mu_t \left(\frac{\partial u_k}{\partial x_k}\right)^2 - \frac{2}{3}\rho k \frac{\partial u_k}{\partial x_k} \tag{10}$$

$$= 2\mu_t S_{ij} S_{ij} - \frac{2}{3}\mu_t \left(\frac{\partial u_k}{\partial x_k}\right)^2 - \frac{2}{3}\rho k \frac{\partial u_k}{\partial x_k} \tag{11}$$

$$= 2\mu_t \overline{S}_{ij} \overline{S}_{ij} - \frac{2}{3}\rho k \frac{\partial u_k}{\partial x_k} \tag{12}$$

where $\overline{S}_{ij}$ is the traceless form of the strain rate tensor (in 3-D):

$$\overline{S}_{ij} = S_{ij} - \frac{1}{3}\frac{\partial u_k}{\partial x_k}\delta_{ij} \tag{13}$$

2.2 Wilcox 2006

In 1998 Wilcox presented a modified version of the k-ω model [8]. Because it has been superseded, this 1998 version is not described here. A newer form of the Wilcox k-ω model [1, 9], referred to here as Wilcox06, was developed to improve the predictive accuracy compared to the 1988 and 1998 versions for free shear flows and strongly separated flows (and hence be more competitive with the Menter SST model, described in the next section). Wilcox06 is given by:

$$\frac{Dk}{Dt} = \frac{\mathcal{P}}{\rho} - \beta^* \omega k + \frac{\partial}{\partial x_j}\left[(\nu + \sigma_k \nu_t')\frac{\partial k}{\partial x_j}\right] \tag{14}$$

$$\frac{D\omega}{Dt} = \frac{\gamma}{\mu_t}\mathcal{P} - \beta\omega^2 + \frac{\partial}{\partial x_j}\left[(\nu + \sigma_\omega \nu_t')\frac{\partial \omega}{\partial x_j}\right] + \frac{\sigma_d}{\omega}\frac{\partial k}{\partial x_j}\frac{\partial \omega}{\partial x_j} \tag{15}$$

where $\nu_t' = k/\omega$. The eddy viscosity is given by:

$$\mu_t = \rho \frac{k}{\tilde{\omega}} \tag{16}$$

where

$$\tilde{\omega} = \max\left(\omega; C_{lim}\sqrt{\frac{2\overline{S}_{ij}\overline{S}_{ij}}{\beta^*}}\right) \tag{17}$$

and $C_{lim} = 7/8$. The coefficients are $\gamma = 13/25$, $\beta = \beta_0 f_\beta$, $\beta^* = 0.09$, $\sigma_\omega = 0.5$, $\sigma_k = 3/5$, $\sigma_{d0} = 1/8$, $\beta_0 = 0.0708$, and

$$\sigma_d = 0 \qquad \frac{\partial k}{\partial x_j}\frac{\partial \omega}{\partial x_j} \leq 0 \tag{18}$$

$$\sigma_d = \sigma_{d0} \qquad \frac{\partial k}{\partial x_j}\frac{\partial \omega}{\partial x_j} > 0 \tag{19}$$

Also:

$$f_\beta = \frac{1 + 85\chi_\omega}{1 + 100\chi_\omega} \tag{20}$$

$$\chi_\omega = \left|\frac{\Omega_{ij}\Omega_{jk}\hat{S}_{ki}}{(\beta^*\omega)^3}\right| \tag{21}$$

where $\hat{S}_{ki} = S_{ki} - \frac{1}{2}(\partial u_m/\partial x_m)\delta_{kl}$. This form forces $\chi_\omega = 0$ for 2-D flow (both incompressible and compressible). The f_β parameter was added by Wilcox to account for the round-jet/plane-jet anomaly [1]. For boundary layer applications, the vortex stretching parameter χ_ω is sometimes ignored (set to zero), yielding $f_\beta = 1$.

2.3 Menter SST

The two-equation SST model of Menter [10] is written as:

$$\frac{Dk}{Dt} = \frac{\mathcal{P}}{\rho} - \beta^*\omega k + \frac{\partial}{\partial x_j}\left[(\nu + \sigma_k \nu_t)\frac{\partial k}{\partial x_j}\right] \tag{22}$$

$$\frac{D\omega}{Dt} = \frac{\gamma}{\mu_t}\mathcal{P} - \beta\omega^2 + \frac{\partial}{\partial x_j}\left[(\nu + \sigma_\omega \nu_t)\frac{\partial \omega}{\partial x_j}\right] + 2(1-F_1)\frac{\sigma_{\omega 2}}{\omega}\frac{\partial k}{\partial x_j}\frac{\partial \omega}{\partial x_j} \tag{23}$$

The eddy viscosity is given by:

$$\mu_t = \rho\frac{a_1 k}{\max(a_1\omega, \Omega F_2)} \tag{24}$$

where $a_1 = 0.31$, Ω is the magnitude of vorticity, and F_1 and F_2 are blending functions (given below).

The "shear stress transport" (SST) part of the model is based on Bradshaw's assumption that the principal shear stress is proportional to k, via: $\tau_{12} = -\rho a_1 k$. From Eq. (5), the primary term in eddy viscosity models is: $\tau_{12} = -2\mu_t S_{12}$. In adverse pressure gradient boundary layer flows, the standard method often leads to too much eddy viscosity (an overprediction of τ_{12}), inhibiting or delaying separation. In these situations, it is better for the model to choose τ_{12} based on Bradshaw' assumption. Using:

$$\rho a_1 k = 2\mu_t S_{12} \tag{25}$$

we find how to set the eddy viscosity in order to recover values corresponding with Bradshaw's assumption:

$$\mu_t = \frac{\rho a_1 k}{2S_{12}} \approx \frac{\rho a_1 k}{\Omega} \tag{26}$$

Functionally, Eq. (24) chooses the minimum eddy viscosity between the standard one and that dictated by Bradshaw's assumption limited to within the boundary layer region.

In the SST model, there are two sets of coefficients, which are combined using a blending function. The constants for set 1 are $\beta_1^* = 0.09$, $\sigma_{k1} = 0.85$, $\beta_1 = 0.075$, $\sigma_{\omega 1} = 0.5$, and $\gamma_1 = \beta_1/\beta_1^* - \sigma_{\omega 1}\kappa^2/\sqrt{\beta_1^*} \approx 0.55317$. The constants for set 2 are $\beta_2^* = 0.09$, $\sigma_{k2} = 1.0$, $\beta_2 = 0.0828$, $\sigma_{\omega 2} = 0.856$, and $\gamma_2 = \beta_2/\beta_2^* - \sigma_{\omega 2}\kappa^2/\sqrt{\beta_2^*} \approx 0.44035$. The constant κ is defined as $\kappa = 0.41$. Set 1 and set 2 are blended via:

$$\phi = F_1\phi_1 + (1-F_1)\phi_2 \tag{27}$$

and

$$F_1 = \tanh(arg_1^4) \tag{28}$$

$$arg_1 = \min\left[\max\left(\frac{\sqrt{k}}{0.09\omega d}; \frac{500\nu}{d^2\omega}\right); \frac{4\rho\sigma_{\omega 2}k}{CD_{k\omega}d^2}\right] \tag{29}$$

$$CD_{k\omega} = \max\left(2\rho\sigma_{\omega 2}\frac{1}{\omega}\frac{\partial k}{\partial x_j}\frac{\partial \omega}{\partial x_j}; 10^{-20}\right) \tag{30}$$

where d is the distance to the nearest wall. The F_2 term is given by:

$$F_2 = \tanh(arg_2^2) \tag{31}$$

$$arg_2 = \max\left(2\frac{\sqrt{k}}{0.09\omega d}; \frac{500\nu}{d^2\omega}\right) \tag{32}$$

2.4 Other Considerations for k-ω Models

For situations in which compressibility is important (and shocks may be present), the turbulence equations are sometimes solved in conservation form. For example, making use of the continuity equation $\partial\rho/\partial t + \partial(\rho u_j)/\partial x_j = 0$, Eqs. (1) and (2) can be written:

$$\frac{\partial(\rho k)}{\partial t} + \frac{\partial(\rho u_j k)}{\partial x_j} = \mathcal{P} - \beta^*\rho\omega k + \frac{\partial}{\partial x_j}\left[(\mu + \sigma_k\mu_t)\frac{\partial k}{\partial x_j}\right] \tag{33}$$

$$\frac{\partial(\rho\omega)}{\partial t} + \frac{\partial(\rho u_j \omega)}{\partial x_j} = \frac{\gamma\rho}{\mu_t}\mathcal{P} - \beta\rho\omega^2 + \frac{\partial}{\partial x_j}\left[(\mu + \sigma_\omega\mu_t)\frac{\partial \omega}{\partial x_j}\right] \tag{34}$$

It is unclear whether the turbulence model equation form (conservative vs. non-conservative) makes much difference in the common situation where the turbulence models are solved separately (loosely coupled) from the conservative mean flow equations. But certainly if the equations are fully coupled, all should be solved consistently in conservation form.

For flows in which the turbulent kinetic energy is non-negligible compared to the square of the mean velocity, the k contributes to the conservation of total energy via $\rho E = \rho(e + \frac{1}{2}u_i u_i + k)$ (see Wilcox [1]). Also, the molecular and turbulent diffusion of k, typically modeled as

$$\frac{\partial}{\partial x_j}\left[(\mu + \sigma_k\mu_t)\frac{\partial k}{\partial x_j}\right] \tag{35}$$

in the mean flow energy equation [11], should be included. Furthermore, the perfect gas equation of state then becomes [12]: $p = (\gamma - 1)\rho(E - \frac{1}{2}u_i u_i - k)$. Because many CFD codes include other (simpler) turbulence models beside two-equation models, for which k is not available, the turbulent kinetic energy contribution to total energy (and its explicit appearance in the energy equation and equation of state) is often ignored.

In an often-used variant of the k-ω model, the production term is simplified by an approximation that makes use of the local magnitude of vorticity Ω:

$$\mathcal{P} = \mu_t\Omega^2 - \frac{2}{3}\rho k\delta_{ij}\frac{\partial u_i}{\partial x_j} = \mu_t\Omega^2 - \frac{2}{3}\rho k\frac{\partial u_k}{\partial x_k} \tag{36}$$

This vorticity source term is often a good approximation of the exact source term in boundary layer flows [13], and its use can avoid some numerical difficulties sometimes associated with the use of the exact source term. Again, it is often common to ignore the $(2/3)\rho k$ term in the production source of Eq. (36) for many applications, but this may have a non-negligible influence for high-speed flows.

The recommended wall boundary conditions for k-ω models are [10]: $k_{wall} = 0$, $\omega_{wall} = 60\nu/[\beta_1(\Delta d_1)^2]$. In his boundary layer code, Wilcox [1] overwrites the computed value of ω with the theoretical value $\omega \approx 6\nu/(\beta_1 y^2)$ at the first grid point off the surface (for smooth walls), but this method of overwriting field variables rather than specifying boundary conditions is undesirable in general-purpose Navier-Stokes codes. The farfield boundary conditions are more difficult to define with confidence. Part of the problem is that the freestream levels are not preserved; they decay rapidly (both due to the equations themselves as well as due to typically coarse grid spacing in the farfield). This decay, which occurs for k-ε equations as well, makes the local "ambient" levels near

the body a function of the farfield grid extent. In the freestream, the k-ω governing equations dictate that the decay of eddy viscosity occurs according to:

$$\mu_t = \mu_{t,\infty}\left[1 + \beta\omega_\infty \frac{x}{u_\infty}\right]^{1-(0.09/\beta)} \tag{37}$$

where x is the distance from the location where the boundary conditions are set. As discussed in Spalart and Rumsey [14], real flow over external aerodynamic configurations has no reason to obey the decay equations used to calibrate two-equation models in isotropic turbulence. In reality, the kinetic energy (and eddy viscosity) relevant to the aircraft flow varies very little over the size of the typical CFD domain. Thus, the behavior represented by decaying freestream turbulence is not representative of reality. Ref. 14 describes the use of sustaining terms which, when added to the k-ω equations, preserve the freestream levels without decay. Although maintaining freestream turbulence is probably important from the point of view of numerical-transition consistency with grid refinement, at high Reynolds numbers the effect is generally small. Therefore, results in this paper will not use the sustaining terms.

For typical subsonic/transonic/supersonic applications, most CFD application codes have developed their own methodology for setting farfield boundary conditions for k and ω, in order to yield reasonable results across a broad range of problems. For example, in CFL3D (Krist et al. [15]), the boundary conditions are: $k/a_\infty^2 = 9 \times 10^{-9}$ and $\omega\mu_\infty/(\rho_\infty a_\infty^2) = 1 \times 10^{-6}$, which always gives $\mu_{t,\infty}/\mu_\infty = 0.009$. Because the freestream turbulence level, Tu (in percent), is given by:

$$\text{Tu}, \% = 100\sqrt{\frac{2}{3}\frac{k}{u_\infty^2}} \tag{38}$$

this means that a fixed $k/a_\infty^2 = 9 \times 10^{-9}$ yields (for example): Tu $= 0.0387\%$ for $M = 0.2$, 0.0039% for $M = 2.0$, 0.0016% for $M = 5.0$, and 0.0008% for $M = 10.0$. Thus, perhaps, it makes better sense when solving over a broad range of Mach numbers to use a fixed Tu (i.e., fixed k/u_∞^2) in the freestream instead of fixed k/a_∞^2). Otherwise higher Mach number cases will have an even greater tendency to become laminar.

3 Compressibility Corrections

Wilcox [1] describes many of the compressible-flow closure approximations. A few of them are already employed in most compressible flow CFD codes. For example, the Reynolds stress tensor of Eq. (5) is already written appropriately for compressible flows. The most commonly used turbulent heat-flux vector ($q_T = -(\mu_t/Pr_t)\partial h/\partial x_j$, where h is enthalpy and Pr_t is typically around 0.9 for boundary layers), has been in common use in compressible flow CFD codes for many years. However, the models for pressure-diffusion, pressure-dilatation, and pressure-work are all either under development, very little is known, or proposed models are too complex or have not gained wide acceptance (see, e.g., Zeman [16], Grasso and Falconi [17], and Yoshizawa et al. [18]). Many of these compressibility effects are presumed to be small in boundary layers [1]. As a result, most widely-used models do not include them. For example, Sarkar's model for the pressure-dilatation correction in compressible flows [19] is rarely employed for boundary-layer computations. See also Wilcox [1] and Grasso and Falconi [17]. In the Sarkar model, the pressure-dilatation adds the following term to the k-equation (in the k-ε model):

$$(-\alpha_2\mathcal{P} + \alpha_3\rho\varepsilon)M_T^2 \tag{39}$$

where $\alpha_2 = 0.15$ (0.4 in Ref. 17), $\alpha_3 = 0.2$, $M_T = (\sqrt{2k})/a$, and a is the local speed of sound.

On the other hand, the Sarkar/Zeman compressibility corrections for dilatation-dissipation are often employed for jets and free shear mixing layers, in spite of the fact that the reasoning behind

them is fundamentally flawed [1]. See also Sarkar [20]. It turns out that dilatation-dissipation is small or negligible, and mixing-layer compressibility effects likely manifest themselves in the pressure-strain redistribution term. Properly formulated corrections are still being explored. In the mean time, the existing dilatation-dissipation corrections provide the desired trends for mixing layers, albeit for the wrong reasons, and so are still considered useful for those cases. It should also be noted that dilatation-dissipation models typically account for the pressure-dilatation correction [21], so when employing both corrections the coefficient in the dilatation-dissipation model must be reduced by about a factor of two from its standard value [17].

Unfortunately, the Sarkar/Zeman compressibility corrections can have a detrimental effect on many boundary-layer predictions (they tend to produce wall skin frictions that are too low, and can also negatively impact the size of the predicted separation region [22]). Wilcox [1, 23] developed a modification that significantly decreases this detrimental effect, and Brown [24] further attempted to eliminate its potential impact in very high Mach number boundary layers by combining it with the F_1 function of Menter (Eq. (28)). In the Wilcox correction, the coefficients of the k-ω destruction terms are modified as follows:

$$\beta_c^* = \beta^* \left[1 + \xi^* F(M_T)\right] \tag{40}$$

$$\beta_c = \beta - \beta^* \xi^* F(M_T) \tag{41}$$

where

$$F(M_T) = \left(M_T^2 - M_{T_0}^2\right) \mathcal{H}\left(M_T - M_{T_0}\right) \tag{42}$$

and $\xi^* = 2$, $M_{T_0} = 0.25$, $M_T = (\sqrt{2k})/a$, $\mathcal{H}(\cdot)$ is the Heaviside function, and a is the local speed of sound.

However, it has been observed [1] that for cold-wall cases the skin friction is typically overpredicted to such an extent that including a dilatation-dissipation correction can yield improved results, although possibly for the wrong reasons. Zeman [16] noted that the apparent unimportance of the pressure-dilatation and dilatation-dissipation in boundary layers is "only a question of degree." He found that as freestream Mach number increases and wall cooling increases, compressibility effects become increasingly important. In the Zeman dilatation-dissipation correction for boundary layers, the coefficients of the k-ω destruction terms are modified as in Eqs. (40) and (41), only now $F(M_T)$ is given by:

$$F(M_T) = \left[1 - \exp\left(-\left(\frac{M_T - M_{T_0}}{\Lambda}\right)^2\right)\right] \mathcal{H}\left(M_T - M_{T_0}\right) \tag{43}$$

with $\xi^* = 0.75$, $M_{T_0} = 0.2$, and $\Lambda = 0.66$.

In addition to a pressure-dilatation correction and a dilatation-dissipation correction, Grasso and Falconi [17] also included a correction to the k-equation in their k-ε model, due to the scalar product of the Favre-velocity and the mean pressure gradient. They believed that this term may be influential in regions of large pressure and density gradients.

Both Wilcox [1] and Huang et al. [25] mention that the k-ε form of the two-equation model exhibits more deviation from the compressible law-of-the-wall than k-ω at high Mach numbers. Wilcox also points out that the k-ε form is more problematic for adverse pressure-gradient wall-bounded flows. Huang et al. proposed a possible iterative procedure to reproduce the expected profile, and also mentioned that alternative forms such as k-$(\varepsilon^{5/6}/k)$ may reduce the sensitivity, but neither of these proposals were widely used.

Catris et al. [26] extended the analysis of Huang et al. [25], and showed that specific corrections to the diffusion terms are necessary to make the models consistent with the logarithmic law for

[1] White, J. A., private communication 2008.

compressible boundary layers. The corrections were derived for a variety of models. Here, we are only concerned with the k-ω form. For example, Eqs. (33) and (34) get altered as follows:

$$\frac{\partial(\rho k)}{\partial t} + \frac{\partial(\rho u_j k)}{\partial x_j} = \mathcal{P} - \beta^* \rho\omega k + \frac{\partial}{\partial x_j}\left[\frac{1}{\rho}\left(\mu + \sigma_k \mu_t\right)\frac{\partial(\rho k)}{\partial x_j}\right] \tag{44}$$

$$\frac{\partial(\rho\omega)}{\partial t} + \frac{\partial(\rho u_j \omega)}{\partial x_j} = \frac{\gamma\rho}{\mu_t}\mathcal{P} - \beta\rho\omega^2 + \frac{\partial}{\partial x_j}\left[\frac{1}{\sqrt{\rho}}\left(\mu + \sigma_\omega \mu_t\right)\frac{\partial(\sqrt{\rho}\omega)}{\partial x_j}\right] \tag{45}$$

where the only changes are in the diffusion terms. However, Catris et al. point out that for k-ω, the difference in results due to modifying the diffusion terms is only very slight. This further confirms the low sensitivity of k-ω to compressibility effects in boundary layer flow, as described in Refs. 1 and 25.

A length-scale modification was proposed by Vuong and Coakley [27] and Huang and Coakley [28], to reduce the magnitude of heat transfer for high-speed separated boundary layers near reattachment. See also Brown [24] and Coratekin et al. [29]. In this correction, the length scale going into the eddy viscosity is limited based on Bradshaw's relation $\tau_t/\rho \propto a_1 k$ and the mixing length relation $\ell = \kappa d$. The turbulent length scale is limited by:

$$\ell = \min\left(\kappa d\sqrt{a_1}; \frac{\sqrt{k}}{\omega}\right) \tag{46}$$

(Note that in Vuong and Coakley and Huang and Coakley, there is an additional factor of $C_\mu = 0.09$ present due to the different way that ω is defined.) Because $\omega = \sqrt{k}/\ell$, the end result is that the eddy viscosity is limited according to:

$$\mu_t = \min\left(\mu_{t,std}; \rho\kappa d\sqrt{a_1 k}\right) \tag{47}$$

where $\mu_{t,std}$ is the eddy viscosity computed the usual way, via Eq. (3), (16), or (24). It should be noted here that the assumption of constant turbulent Prandtl number has been recently questioned, relative to its effect on heat flux for shock/boundary layer cases [30]. A variable turbulent Prandtl number model was shown to improve heat flux near reattachment.

A rapid compression fix was implemented by Coakley and Huang [31] (see also Vuong and Coakley [27], Coratekin et al. [29], and Forsythe et al. [32]). In this fix, the production term in the ω-equation

$$\frac{\gamma\rho}{\mu_t}\mathcal{P} = -\frac{\gamma\rho}{\mu_t}\tau_{ij}\frac{\partial u_i}{\partial x_j} = \frac{\gamma\rho}{\mu_t}\left[\mu_t\overline{S}^2 - \frac{2}{3}\rho k\delta_{ij}\frac{\partial u_i}{\partial x_j}\right] \tag{48}$$

$$= \gamma\rho\overline{S}^2 - \frac{2}{3}\gamma\rho\omega\frac{\partial u_k}{\partial x_k} \tag{49}$$

is altered to read:

$$\frac{\gamma\rho}{\mu_t}\mathcal{P} = \gamma\rho\overline{S}^2 - \frac{4}{3}\rho\omega\frac{\partial u_k}{\partial x_k} \tag{50}$$

where

$$\overline{S}^2 \equiv \left(\frac{\partial u_i}{\partial x_j} + \frac{\partial u_j}{\partial x_i} - \frac{2}{3}\frac{\partial u_k}{\partial x_k}\delta_{ij}\right)\frac{\partial u_i}{\partial x_j} = \left(\frac{\partial u_i}{\partial x_j} + \frac{\partial u_j}{\partial x_i}\right)\frac{\partial u_i}{\partial x_j} - \frac{2}{3}\left(\frac{\partial u_k}{\partial x_k}\right)^2 = S^2 - \frac{2}{3}\left(\frac{\partial u_k}{\partial x_k}\right)^2 \tag{51}$$

or equivalently:

$$\overline{S}^2 = 2\overline{S}_{ij}\overline{S}_{ij} \tag{52}$$

where $\overline{S}_{ij}$ was defined earlier in Eq. (13). Thus, in this rapid compression fix, the original $(2/3)\gamma$ (which is close to $1/3$) gets increased to a fixed value of $4/3$ for linear deformations.

This modification was made in order to increase the size of computed separation bubble regions, by insuring that the turbulent length scale does not change too quickly when undergoing rapid compression. However, as discussed in Forsythe et al. [32], the shear-stress transport part of the Menter SST model already improves correlations with experimental bubble size, so the ad hoc rapid compression fix was not used for that model. The Wilcox06 model is designed with a similar stress limiter modification, so this model, too, probably would not benefit from the rapid compression fix.

In summary, when considering high Mach number compressible boundary layer flows using k-ω models, the conservation of total energy should be configured to include the contribution of the turbulent kinetic energy k, and the mean flow energy equation should include the molecular and turbulent diffusion of k. It is sometimes common practice to ignore these effects, which is certainly justified when k is significantly smaller than the square of the mean velocity. Furthermore, turbulent production should officially include the $(2/3)\rho k$ term, which multiplies $\partial u_k/\partial x_k$ and hence is identically zero for incompressible flows. Because this term typically has little effect over a broad range of conditions, it is sometimes ignored, particularly when other approximations, limiting, etc. are employed for turbulence production. Other than these considerations (which may or may not be important, depending on the case), little extra appears to be called for – based on the currently available literature – in terms of specific corrections for compressible Navier-Stokes codes applied to boundary layer flows. Adopting the modified diffusion-term form of Catris et al. [26] has been shown to make very little difference for k-ω models. The length-scale modification of Vuong and Coakley [27] appears to only be important for the specific circumstance of predicting heat transfer near reattachment after separation, but this flow feature may also be improved by adopting models with variable turbulent Prandtl number. The rapid compression fix of Coakley and Huang [31] has been negated by the more accepted stress limiters that appear in SST and Wilcox06.

However, Zeman [16] and practical experience indicates that the need for corrections in hypersonic boundary layers becomes increasingly evident as Mach number increases, particularly for cold walls. But the "traditional" Sarkar / Zeman / Wilcox fixes for free shear flows tend to over-correct in many cases when applied to boundary layer flows. In the Results section, the influence of the less-widely-used Zeman correction (formulated for boundary layer flows) is explored.

4 Results

4.1 Experimental Correlations for Skin Friction and Heat Transfer on a Flat Plate

Wall skin friction is given by the formula:

$$C_f = \frac{\tau_w}{2\rho_e U_e^2} \tag{53}$$

where τ_w is the wall shear stress $\mu_w \partial u/\partial y|_w$ and the subscript "e" represents "edge" or freestream values. There have been a plethora of correlations for wall skin friction (and heat transfer) for the flat plate over the years. See, for example, White [33], Peterson [34], and Hopkins and Inouye [35]. One of the reasons for the large number is the fact that there is a significant amount scatter in the available experimental data, especially those with heat transfer, making certainty difficult. Many of the skin friction correlations use a compressibility transformation idea:

$$C_f = \frac{1}{F_c} C_{f,\mathrm{incomp}}(Re_\theta F_{Re_\theta}) \tag{54}$$

In other words, the formula for incompressible $C_{f,\mathrm{incomp}}$, which is often expressed as a function of Re_θ, is instead computed using the altered variable $Re_\theta F_{Re_\theta}$, and then divided by the function F_c. A widely-used correlation for $C_{f,\mathrm{incomp}}$ is the Karman-Schoenherr relation (see Roy and Blottner [36]):

$$C_{f,\mathrm{incomp}} = \frac{1}{\log_{10}\left(2Re_\theta\right)\left[17.075\log_{10}\left(2Re_\theta\right)+14.832\right]} \tag{55}$$

Here, we examine three correlations for C_f: van Driest [37], Spalding and Chi [38], and White and Christoph [33]. For each of these, the F_c is defined the same way:

$$F_c = \frac{T_{aw}/T_e - 1}{\left(\sin^{-1}A + \sin^{-1}B\right)^2} \tag{56}$$

where T_e represents the "edge" or freestream temperature, and

$$T_{aw} = T_e\left(1 + r\frac{\gamma-1}{2}M^2\right) \tag{57}$$

The recovery factor r is taken to be 0.9. This empirical factor is often introduced because in practice energy recovery is not perfect. The numerator of Eq. (56) is thus simply $\frac{1}{2}r(\gamma-1)M^2$. The A and B are given by:

$$A = \frac{2a^2-b}{\left(b^2+4a^2\right)^{1/2}} \tag{58}$$

$$B = \frac{b}{\left(b^2+4a^2\right)^{1/2}} \tag{59}$$

where

$$a = \left(r\frac{\gamma-1}{2}M^2\frac{T_e}{T_w}\right)^{1/2} \tag{60}$$

$$b = \frac{T_{aw}}{T_w} - 1 = \frac{T_e}{T_w}\left(1 + r\frac{\gamma-1}{2}M^2\right) - 1 \tag{61}$$

A contour plot of F_c as a function of Mach number and $\log_{10}(T_w/T_e)$ is shown in Fig. 1. A different version of this same plot is also given in Spalding and Chi [38].

The three correlations differ in their definitions of F_{Re_θ}:

$$F_{Re_\theta} = \frac{\mu_e}{\mu_w} \qquad \text{van Driest} \tag{62}$$

$$F_{Re_\theta} = \left(\frac{T_w}{T_e}\right)^{-0.702}\left(\frac{T_{aw}}{T_w}\right)^{0.772} \qquad \text{Spalding and Chi} \tag{63}$$

$$F_{Re_\theta} = \sqrt{F_c}\left(\frac{\mu_e}{\mu_w}\right)\left(\frac{T_e}{T_w}\right)^{1/2} \text{White and Christoph} \tag{64}$$

(Note the typographical error in White [33] in Table 7-3, where the term Q is inverted.) Both van Driest and White/Christoph correlations are functions of μ_e/μ_w. This quantity can be obtained via Sutherland's law (see White [33]):

$$\mu = \mu_0\left(\frac{T}{T_0}\right)^{3/2}\frac{T_0+S'}{T+S'} \tag{65}$$

where for air $\mu_0 = 0.1716$ mP, $T_0 = 491.6$ R, and $S' = 199$ R. Thus:

$$\frac{\mu_e}{\mu_w} = \left(\frac{T_w}{T_e}\right)^{-3/2} \frac{(T_w/T_e) + (S'/T_e)}{1 + (S'/T_e)} \tag{66}$$

Therefore, when Sutherland's law is used, both of these correlations are functions not only of the ratio T_w/T_e, but also of the freestream temperature T_e itself. For all of the work herein, T_e is chosen to be 540 R. Contour plots of F_{Re_θ} for the three correlations are shown in Figs. 2(a) - (c). Note that a different version of Fig. 2(b) can also be found in Spalding and Chi [38].

Using Eq. (55) for the $C_{f,\text{incomp}}$ value, results for the compressible C_f can be computed for each of the correlations. It turns out that results using van Driest and White/Christoph are very similar, so only the results of van Driest and Spalding/Chi are shown in Fig. 3 for clarity of presentation. Plots of $C_f/C_{f,\text{incomp}}$ are shown here for a variety of T_w/T_e ratios, as well as for adiabatic wall temperature. In all cases, an assumed Re_x of 5×10^6 was used. In terms of Re_θ, this translates to approximately $Re_\theta = 14200$, using the formula $Re_\theta \approx 0.0142 Re_x^{6/7}$ from White [33]. For the adiabatic case (for which the most experimental data exist), the correlations give nearly the same result (black lines). But for fixed wall temperature ratios, the results can differ significantly. Spalding and Chi [39] claim a smaller root mean square error compared to van Driest [37] using a variety of experiments, but recall that relatively few experiments exist for walls with heat transfer. Plots of compressible C_f vs. Re_x are shown in Figs. 4(a) and (b) for several specific cases. In Fig. 4(a), the results of the correlations agree well, whereas in Fig. 4(b) the correlations are seen to differ by as much as 50% or more. The main point here is that there is some uncertainty regarding C_f for walls with heat transfer, so it is more difficult to validate (or invalidate) turbulence models for these cases with confidence. In the literature, most people tend to compare with the van Driest correlation, but others have since developed correlations that may work better in specific cases. For example, Huang et al. [40] developed a method for which skin friction for strongly cooled walls falls below van Driest, in better agreement with data.

The wall heat flux is often expressed [33] in terms of the Stanton number:

$$St = C_h = \frac{q_w}{\rho_e U_e c_p (T_{aw} - T_w)} \tag{67}$$

where the heat flow at the wall $q_w = -k(\partial T/\partial y)|_w$. The so-called Reynolds analogy is usually used to relate the local wall heat flux in terms of skin friction:

$$St \approx \frac{1}{2} C_f R_{af} \tag{68}$$

where R_{af} is the Reynolds analogy factor. This factor generally lies in the range $0.9 < R_{af} < 1.3$, and is believed to be close to unity for hypersonic flows [36] and for very cold walls [22]. Thus, St is directly proportional to C_f, at approximately half its numerical value (with appropriate sign).

4.2 CFD Results on a Flat Plate

In order to test the ability of k-ω turbulence models to predict compressible boundary layer flow, computations were performed for flow over a flat plate in zero pressure gradient for a variety of flow conditions. Most of the computations were performed using the CFL3D code [15]. Note that in CFL3D, the turbulence models are decoupled from the mean flow equations, k is *not* included in the definition of total energy, and diffusion of k does not appear in the mean flow energy equation for its models tested here. Furthermore, for the current applications, Eq. (36) is used for production, with the $(2/3)\rho k$ term ignored. (Some computations were tried with this term included, and it was found to make little difference even for $M = 10$ cases.) The $(2/3)\rho k$ term was also neglected in τ_{ij}, Eq. (5). For comparison, several results were also obtained using the VULCAN code [41], in which the turbulence models are fully coupled to the mean flow equations and no approximations are made for τ_{ij} or the turbulence production terms.

Table 1. Flat plate cases computed

Mach	T_w/T_∞	$T_w/T_{aw,ideal}$	wall type
0.2	1.008	1.0	adiabatic
5.0	6.0	1.0	adiabatic
10.0	21.0	1.0	adiabatic
0.2	5.0	4.96	hot
2.0	1.0	0.556	cold
2.0	2.0	1.11	hot
5.0	1.0	0.167	cold
5.0	3.0	0.5	cold
5.0	20.0	3.33	hot
10.0	1.0	0.0476	cold
10.0	10.0	0.476	cold
10.0	40.0	1.905	hot

The majority of runs were performed using the Menter SST model. Full Navier-Stokes (as opposed to thin-layer) was employed. For subsonic Mach numbers, the inflow boundary condition set total pressure and total temperature conditions (according to the particular Mach number). The pressure was extrapolated from the interior of the domain, and the remaining variables were determined from the extrapolated pressure and the input data, using isentropic relations. The outflow boundary condition set $p/p_\infty = 1$ and extrapolated all other quantities from the interior of the domain. For supersonic Mach numbers, the inflow boundary condition set all primitive variables, and the outflow boundary condition extrapolated all variables from the interior of the domain. In all cases the top boundary, located a nondimensional distance $y = 1$ from the wall, used a farfield Riemann invariant boundary condition. The wall boundary condition enforced no slip, and set temperature either (1) according to a desired T_w/T_∞, or (2) according to $T_w = T_{aw,ideal}$, where $T_{aw,ideal}$ is the ideal adiabatic wall temperature computed from $T_{aw,ideal} = T_\infty(1 + \frac{1}{2}(\gamma - 1)M^2)$. This latter method yielded almost the same results as enforcing zero wall temperature gradient, which insured no heat flux at the wall. The freestream T_∞ was taken to be 540 R.

As mentioned earlier, the wall boundary conditions for turbulent quantities were those recommended by Menter [10]. Although not shown, the boundary condition on ω_{wall} was varied by a factor of 10 in both directions, but this change did not have an appreciable influence on the results. The farfield boundary conditions for turbulent quantities were determined from $\mathrm{Tu} = 0.08165\%$ and $\mu_{t,\infty}/\mu_\infty = (2 \times 10^{-7})Re$. For the results to be shown, $Re = 10^7$ over the length of a plate 2 nondimensional units long. Thus, Re per unit length was 5×10^6 and $\mu_{t,\infty}/\mu_\infty = 1.0$.

The finest grid employed was 273×193, with 225 points on the plate and 49 points leading up to the plate (where symmetry was imposed). Nondimensional minimum normal spacing at the wall was approximately $\Delta y = 1 \times 10^{-6}$, yielding average $y^+ = 0.2$ (or less for higher Mach numbers). There was streamwise clustering near the plate leading edge, as shown in Fig. 5, for which only every fourth grid point is shown for clarity. For supersonic Mach number cases, it was necessary to employ a flux limiter in the computations.

Table 1 summarizes the cases computed. For the purposes of this study, the wall temperature is defined as "hot" or "cold" depending on whether it is above or below the ideal adiabatic wall temperature. Note that the $M = 2$, $T_w/T_\infty = 2$ case is only slightly hot, with wall temperature only slightly above adiabatic.

A grid study for the $M = 5$ adiabatic wall case was conducted using the SST model on the 273×193 (fine grid), along with two successively coarser grids for which every other grid point was removed in each coordinate direction (medium: 137×97; coarse: 69×49). Results are shown in Fig. 6. The biggest differences were near the plate leading edge, particularly for the coarse level. But

over most of the plate the medium and fine grids yielded very close results. For example, between $Re_x = 5 \times 10^6$ and the trailing edge of the plate, the C_f results on the medium and fine grids differed by less than 0.2%.

In order to get an idea about the magnitude of the computed turbulent kinetic energy relative to the square of the velocity, profiles of local k/U^2 are shown as a function of y in the boundary layer at the x-location where $Re_x = 5 \times 10^6$ for several different cases in Fig. 7(a). The maximum level was only about 3%. Fig. 7(b) shows the value of another quantity sometimes used to ascertain the compressibility effects of turbulence (albeit most commonly for free shear layer applications) [21], the turbulence Mach number $M_T = (\sqrt{2k})/a$, where a is the local speed of sound. The highest levels in the boundary layer at a given freestream Mach number occur for the cold-wall cases. For example, for $M = 10$, $T_w/T_\infty = 1$, the peak M_T reaches approximately 0.5.

Results for the adiabatic wall cases using the finest grid are shown in comparison with van Driest and Spalding/Chi correlations in Fig. 8. The CFD results captured the correct trends compared to theory, although the tendency of numerically-induced transition in the CFD to occur further aft with increasing Mach number should be noted [42]. Compared to the correlations, the SST model slightly underpredicted turbulent skin friction for the subsonic Mach number case and overpredicted the correlations for the hypersonic Mach numbers. The Wilcox06 model produced similar C_f as SST for all three cases, although it had a greater tendency to remain laminar than SST as the Mach number increased. (Although not shown, increasing freestream Tu could shift the transition location for Wilcox06 forward.)

Effects of a different code (VULCAN with SST model), as well as effects of including two different compressibility corrections, are shown in Fig. 9. The VULCAN results are seen to be relatively close to the CFL3D results on the same grid, yielding slightly lower C_f levels. Regarding the compressibility corrections, generally speaking, for adiabatic wall with freestream $M \leq 10$ there is only a fairly small influence on the results. Both the Wilcox and the Zeman corrections reduce the skin friction, with the Wilcox correction having the larger effect. Note that Wilcox [1] reported a larger decrease in C_f with the Zeman correction because he used different coefficients (his version of the Zeman model was designed for free shear flows).

Results for two cold-wall cases are shown in Fig. 10. Again, both CFL3D and VULCAN (using SST) yield skin friction levels that are very close. These SST results are significantly high in comparison with the correlations. It is generally well-known that simple algebraic turbulence models such as Baldwin-Lomax [43] can perform reasonably well for attached hypersonic boundary layer flows, provided that the definition of y^+ in the van Driest damping function uses local values for ρ and μ (rather than wall values) [44], as follows: $y^+ = \sqrt{(\rho\tau_w)}y/\mu$. As shown here, using this version of Baldwin-Lomax for the two cold-wall cases yields better predictions than SST, in reasonably good agreement with the van Driest correlation. Employing SST with the Wilcox compressibility correction (SST + Wilcox cc) lowers skin friction significantly. Both CFL3D and VULCAN produce nearly identical results. Although results still lie within the band defined by the two correlations, the SST + Wilcox cc results are quite a bit lower than those of Baldwin-Lomax. Results with the Zeman correction agree better with Baldwin-Lomax results and the van Driest correlation. As shown in Fig. 11, the Baldwin-Lomax model and SST + Zeman cc produce lower eddy viscosity values than uncorrected SST very near the wall (corresponding to $y^+ < O(100)$). The lower levels produce a "less turbulent" profile, and consequently lower wall skin friction.

Results for two hot-wall cases are shown in Fig. 12. In these cases, the results using SST generally fell within the shaded band defined by the two correlations; for $M = 0.2$, $T_w/T_\infty = 5$ results were closer to the van Driest correlation, and for $M = 5$, $T_w/T_\infty = 20$ results were closer to the Spalding/Chi correlation. For these cases, the compressibility corrections made almost no difference in the results.

Using the same plot format shown earlier in Fig. 3, CFD results using the SST model (without and with the Zeman compressibility correction) for various cases in terms of the ratio $C_f/C_{f,\mathrm{incomp}}$ are over-plotted alongside the correlations for $Re_x = 5 \times 10^6$ in Figs. 13(a) and (b). In all cases the $C_{f,\mathrm{incomp}}$ used was the CFD result for $M = 0.2$ with adiabatic wall temperature. The SST results

are given by the large filled-in symbols. The trends discussed above can be clearly discerned in this plot. Although overall the general effects of Mach number and wall temperature on skin friction can be *qualitatively* predicted by SST with no explicit compressibility correction, Fig. 13(a) shows that adiabatic and cold-wall cases are consistently overpredicted *quantitatively* as Mach number is increased (up to about 30% at $M = 10$ for adiabatic walls, and up to as much as $40 - 100\%$ at $M = 10$ for cold walls). On the other hand, hot-wall cases yielded results that lay in or near the band defined by the two correlations. Fig. 13(b) shows that SST results using the Zeman compressibility correction are significantly closer to the correlations.

Results can also be plotted as a function of $T_w/T_{aw,ideal}$. Fig. 14 shows van Driest and Spalding/Chi correlations for both $M = 5$ and $M = 10$, along with current SST results. The SST results with no compressibility correction mostly lie above the shaded regions defined by the two correlations, except for the hot wall cases where results start to fall below the Spalding/Chi correlation. When the Zeman compressibility correction is employed, cold wall results are improved relative to the correlations, while hot wall results are essentially not changed at all.

5 Conclusions

The most widely-used compressibility corrections for k-ω models for high Mach number boundary layer flows are based on improvements intended for free shear applications. As such, these corrections are often unacceptable for boundary layer flows, and many researchers prefer to employ no corrections at all. Although it should be borne in mind that there is some uncertainty in the theoretical correlations (especially at Mach numbers well above 5), it appears that the uncorrected k-ω models perform progressively worse – particularly for cold walls – as the Mach number is increased in the hypersonic regime. As is well-known, simple algebraic models such as Baldwin-Lomax perform better compared to experiment and correlations in these circumstances.

There is still no clarity about whether dilatation-dissipation and pressure-dilatation effects are important in boundary layers or not, particularly at the higher Mach numbers and for cold-wall hypersonic cases. Anything that reduces near-wall eddy viscosity in these situations can help obtain better agreement with correlations, but there is currently no strong physical argument for choosing one "fix" over another. Corrections designed for improving free shear flows tend to over-correct in the boundary layer and yield wall skin friction (and heat transfer) values that are too low. In this paper, it was shown that a dilatation-dissipation correction designed by Zeman specifically for use in boundary layer flows works reasonably well for cold wall cases. Its influence is smaller in the boundary layer than the popular Wilcox correction.

The physical modeling needed to improve wall skin friction predictions in highly compressible boundary layer flows has yet to be formulated and accepted for k-ω turbulence models. Currently, omitting explicit compressibility corrections works reasonably well only for lower Mach numbers (e.g., $M < 5$) or for hot-wall cases. Using the Zeman compressibility correction (formulated for boundary layers) improves high-Mach-number cold wall results, but it would be an insufficient correction for free shear flows. Better overall physics-based compressible turbulence modeling is clearly needed.

References

1. Wilcox, D. W., *Turbulence Modeling For CFD*, 3rd ed., DCW Industries, La Canada, 2006.

2. Morkovin, M., "Effects of Compressibility on Turbulent Flows," *Mecanique de la Turbulence*, edited by A. Favre, Gordon and Breach, New York, 1962, pp. 367–380.

3. So, R. M. C., Gatski, T. B., and Sommer, T. P., "Morkovin Hypothesis and the Modeling of Wall-Bounded Compressible Turbulent Flows," *AIAA Journal*, Vol. 36, No. 9, 1998, pp. 1583–1592.

4. Sarkar, S., Erlebacher, G., Hussaini, M. Y., and Kreiss, H. O., "The Analysis and Modeling of Dilatational Terms in Compressible Turbulence," NASA CR-181959, 1989.

5. Aupoix, B., "Modelling of Compressibility Effects in Mixing Layers," *Journal of Turbulence*, Vol. 5, 2004, 007.

6. Abdol-Hamid, K. S., Pao, S. P., Massey, S. J., and Elmiligui, A., "Temperature Corrected Turbulence Model for High Temperature Jet Flow," *Journal of Fluids Engineering*, Vol. 126, No. 5, 2004, pp. 844-850.

7. Wilcox, D. W., *Turbulence Modeling For CFD*, 1st ed., DCW Industries, La Canada, 1994.

8. Wilcox, D. W., *Turbulence Modeling For CFD*, 2nd ed., DCW Industries, La Canada, 1998.

9. Wilcox, D. W., "Formulation of the k-ω Turbulence Model Revisited," *AIAA Journal*, Vol. 46, No. 11, 2008, pp. 2823–2838.

10. Menter, F. R., "Two-Equation Eddy-Viscosity Turbulence Models for Engineering Applications," *AIAA Journal*, Vol. 32, No. 8, 1994, pp. 1598–1605.

11. Baurle, R. A., "Modeling of High Speed Reacting Flows: Established Practices and Future Challenges," AIAA Paper 2004-267, January 2004.

12. Morrison, J. H., "Flux Difference Split Scheme for Turbulent Transport Equations," AIAA Paper 90-5251, October 1990.

13. Menter, F. R., "Improved Two-Equation k-omega Turbulence Models for Aerodynamic Flows," NASA TM 103975, October 1992.

14. Spalart, P. R. and Rumsey, C. L., "Effective Inflow Conditions for Turbulence Models in Aerodynamic Calculations," *AIAA Journal*, Vol. 45, No. 10, 2007, pp. 2544–2553.

15. Krist, S. L., Biedron, R. T., and Rumsey, C. L., "CFL3D User's Manual (Version 5.0)," NASA TM-1998-208444, June 1998.

16. Zeman, O., "A New Model for Supersonic/Hypersonic Turbulent Boundary Layers," AIAA Paper 93-0897, January 1993.

17. Grasso, F. and Falconi, D., "High-Speed Turbulence Modeling of Shock-Wave / Boundary-Layer Interaction," *AIAA Journal*, Vol. 31, No. 7, 1993, pp. 1199–1206.

18. Yoshizawa, A., Liou, W. W., Yokoi, N., and Shih, T.-H., "Modeling of Compressible Effects on the Reynolds Stress using a Markovianized Two-Scale Method," *Physics of Fluids*, Vol. 9, No. 10, 1997, pp. 3024–3036.

19. Sarkar, S., "The Pressure-Dilatation Correlation in Compressible Flows," *Physics of Fluids A*, Vol. 4, No. 12, 1992, pp. 2674–2682.

20. Sarkar, S., "The Stabilizing Effect of Compressibility in Turbulent Shear Flow," *Journal of Fluid Mechanics*, Vol. 282, 1995, pp. 163–186.

21. Chassaing, P., Antonia, R. A., Anselmet, F., Joly, L., and Sarkar, S., *Variable Density Fluid Turbulence*, Kluwer Academic Publishers, Dordrecht, 2002.

22. MacLean, M., Wadhams, T., Holden, M., and Johnson, H., "A Computational Analysis of Ground Test Studies of the HIFiRE-1 Transition Experiment," AIAA Paper 2008-0641, January 2008.

23. Wilcox, D. C., "Progress in Hypersonic Turbulence Modeling," AIAA Paper 91-1785, June 1991.

24. Brown, J., "Turbulence Model Validation for Hypersonic Flows," AIAA Paper 2002-3308, June 2002.

25. Huang, P. G., Bradshaw, P., and Coakley, T. J., "Turbulence Models for Compressible Boundary Layers," *AIAA Journal*, Vol. 32, No. 4, 1994, pp. 735–740.

26. Catris, S. and Aupoix, B., "Density Corrections for Turbulence Models," *Aerospace Science and Technology*, Vol. 4, 2000, pp. 1-11.

27. Vuong, S. T. and Coakley, T. J., "Modeling of Turbulence for Hypersonic Flows with and without Separation," AIAA Paper 87-0286, January 1986.

28. Huang, P. G. and Coakley, T. J., "Turbulence Modeling for Complex Hypersonic Flows," AIAA Paper 93-0200, January 1993.

29. Coratekin, T., van Keuk, J., and Ballmann, J., "Performance of Upwind Schemes and Turbulence Models in Hypersonic Flows," *AIAA Journal*, Vol. 42, No. 5, 2004, pp. 945–957.

30. Xiao, X., Hassan, H. A., Edwards, J. R., and Gaffney, R. L., Jr., "Role of Turbulent Prandtl Numbers on Heat Flux at Hypersonic Mach Numbers," *AIAA Journal*, Vol. 45, No. 4, 2007, pp. 806–813.

31. Coakley, T. J. and Huang, P. G., "Turbulence Modeling for High Speed Flows," AIAA Paper 92-0436, January 1992.

32. Forsythe, J. R., Hoffmann, K. A., and Damevin, H.-M., "An Assessment of Several Turbulence Models for Supersonic Compression Ramp Flow," AIAA Paper 98-2648, June 1998.

33. White, F. M., *Viscous Fluid Flow*, McGraw-Hill Book Company, New York, 1974.

34. Peterson, J. B., Jr., "A Comparison of Experimental and Theoretical Results for the Compressible Turbulent-Boundary-Layer Skin Friction with Zero Pressure Gradient," NASA TN D-1795, March 1963.

35. Hopkins, E. J. and Inouye, M., "An Evaluation of Theories for Predicting Turbulent Skin Friction and Heat Transfer on Flat Plates at Supersonic and Hypersonic Mach Numbers," *AIAA Journal*, Vol. 9, No. 6, 1971, pp. 993–1003.

36. Roy, C. J. and Blottner, F. G., "Review and Assessment of Turbulence Models for Hypersonic Flows," *Progress in Aerospace Sciences*, Vol. 42, 2006, pp. 469–530.

37. Van Driest, E. R., "Problem of Aerodynamic Heating," *Aeronautical Engineering Review*, Vol. 15, October 1956, pp. 26–41.

38. Spalding, D. B. and Chi, S. W., "The Drag of a Compressible Turbulent Boundary Layer on a Smooth Flat Plate With and Without Heat Transfer," *Journal of Fluid Mechanics*, Vol. 18, No. 1, 1964, pp. 117–143.

39. Spalding, D. B. and Chi, S. W., "Skin Friction Exerted by a Compressible Fluid Stream on a Flat Plate," *AIAA Journal*, Vol. 1, No. 9, 1963, pp. 2160–2161.

40. Huang, P. G., Bradshaw, P., and Coakley, T. J., "Skin Friction and Velocity Profile Family for Compressible Turbulent Boundary Layers," *AIAA Journal*, Vol. 31, No. 9, 1993, pp. 1600–1604.

41. White, J. A., and Morrison, J. H., "Pseudo-Temporal Multi-Grid Relaxation Scheme for Solving the Parabolized Navier-Stokes Equations," AIAA Paper 99-3360, June 1999.

42. Rumsey, C. L. and Spalart, P. R., "Turbulence Model Behavior in Low Reynolds Number Regions of Aerodynamic Flowfields," AIAA Paper 2008-4403, June 2008.

43. Baldwin, B. S. and Lomax, H., "Thin-Layer Approximation and Algebraic Model for Separated Turbulent Flows," AIAA Paper 78-257, June 1978.

44. Dilley, A. D., "Evaluation of CFD Turbulent Heating Prediction Techniques and Comparison with Hypersonic Experimental Data," NASA/CR-2001-210837, March 2001.

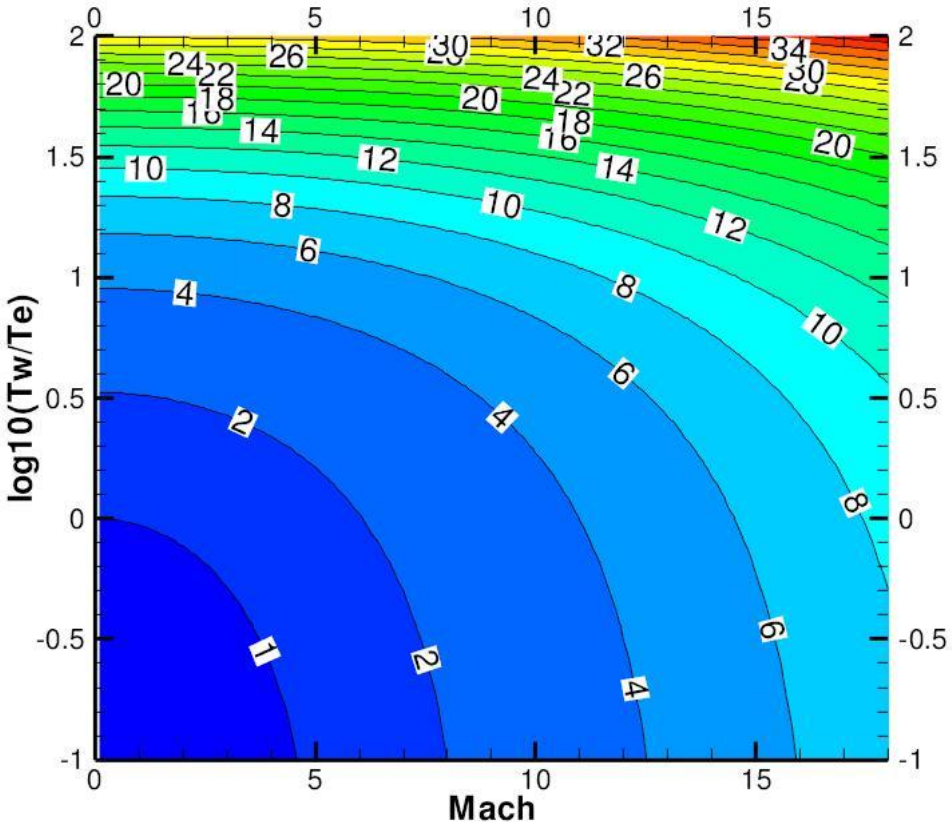

Figure 1. Contours of F_c using Eq. (56).

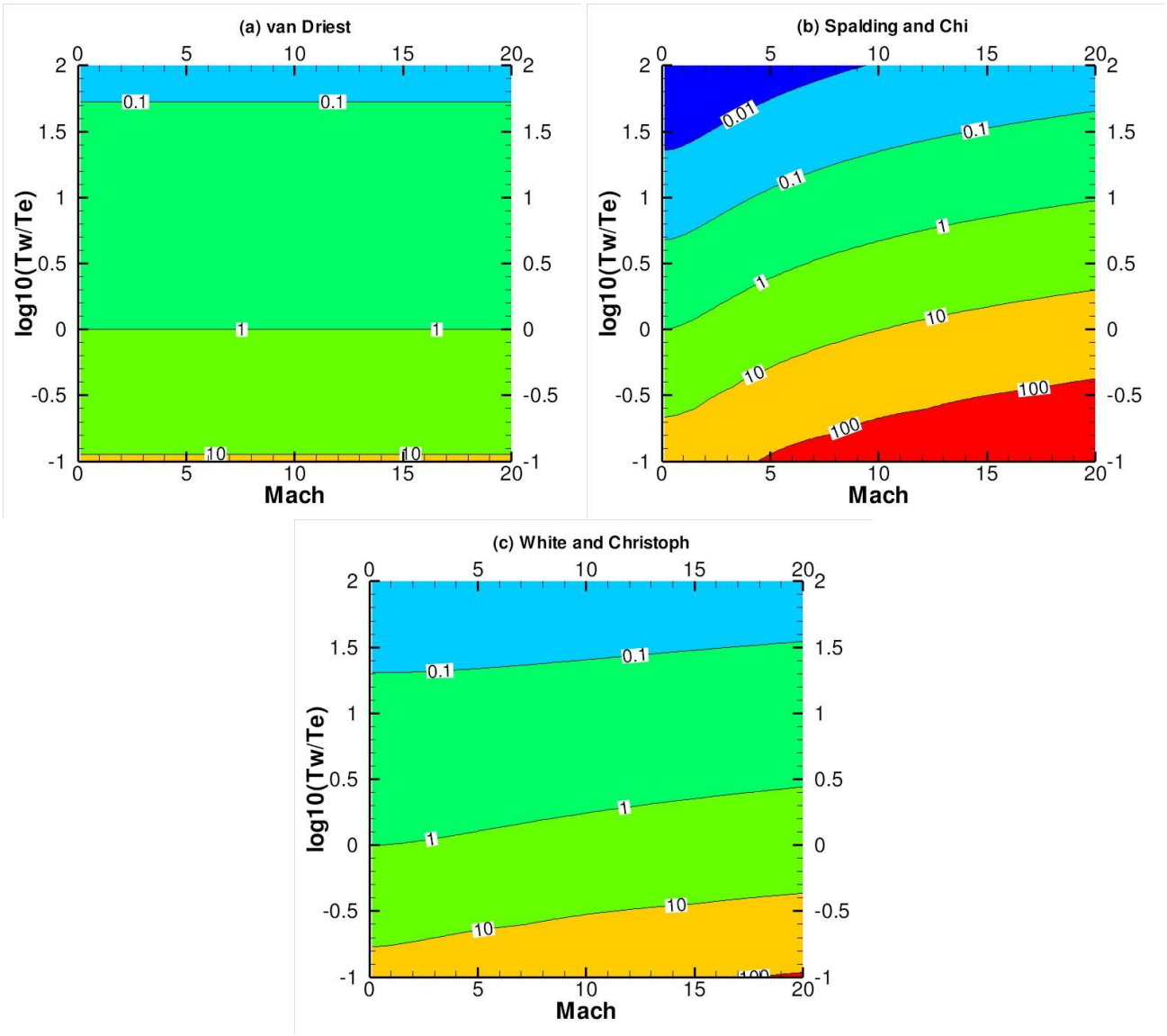

Figure 2. Contours of $F_{Re\theta}$ using (a) Eq. (62), (b) Eq. (63), and (c) Eq. (64).

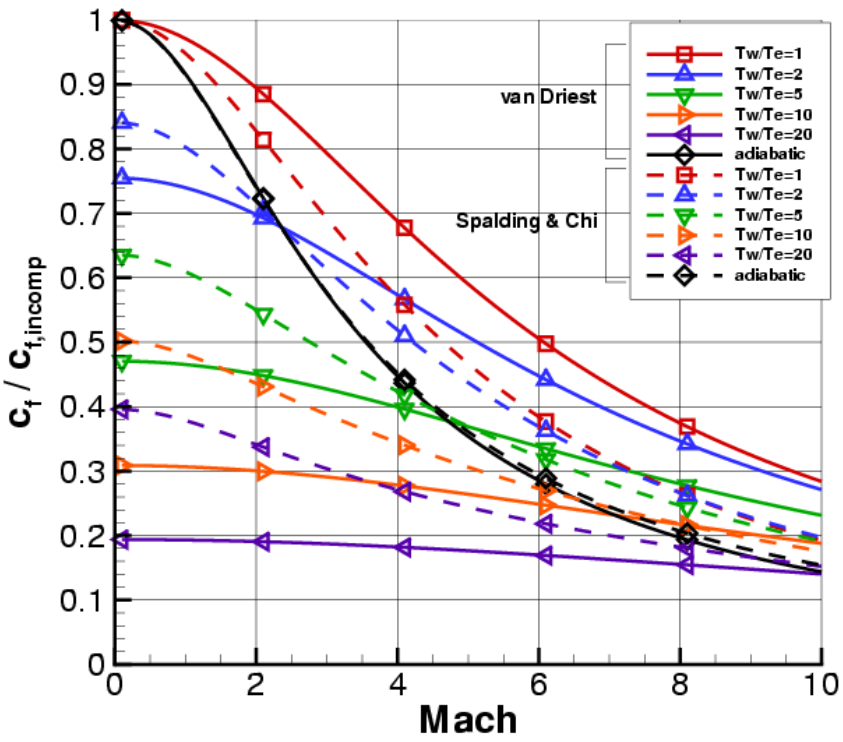

Figure 3. Theoretical compressible wall skin friction compared to incompressible level for $Re_x = 5 \times 10^6$, $T_e = 540$ R, using two different correlations.

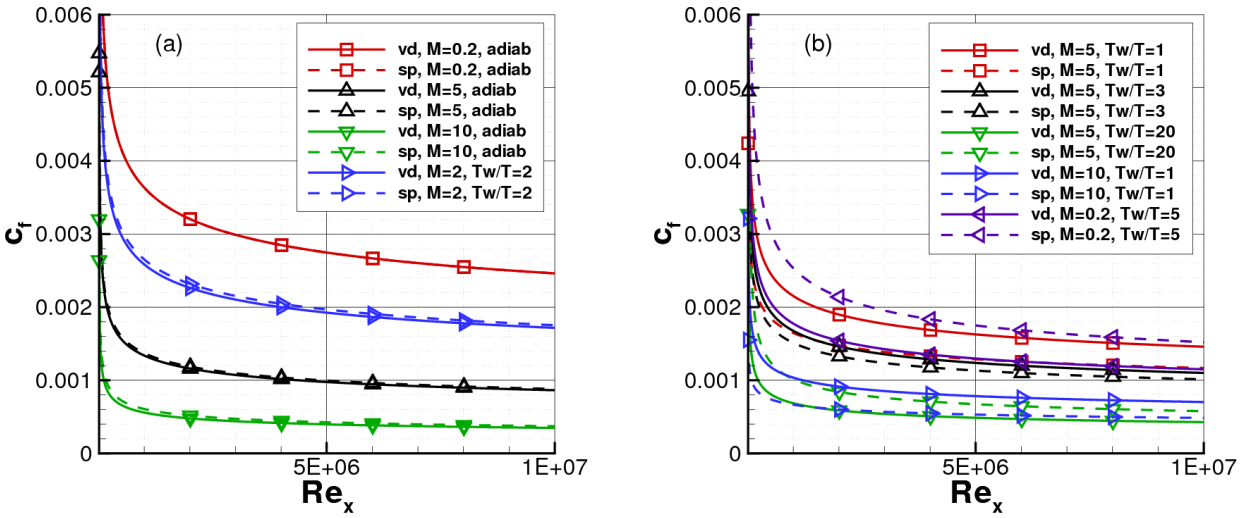

Figure 4. Theoretical values of compressible wall skin friction as a function of Re_x; (a) for selected cases where the van Driest (solid lines) and Spalding/Chi (dashed lines) correlations agree well, (b) for selected cases where the correlations differ.

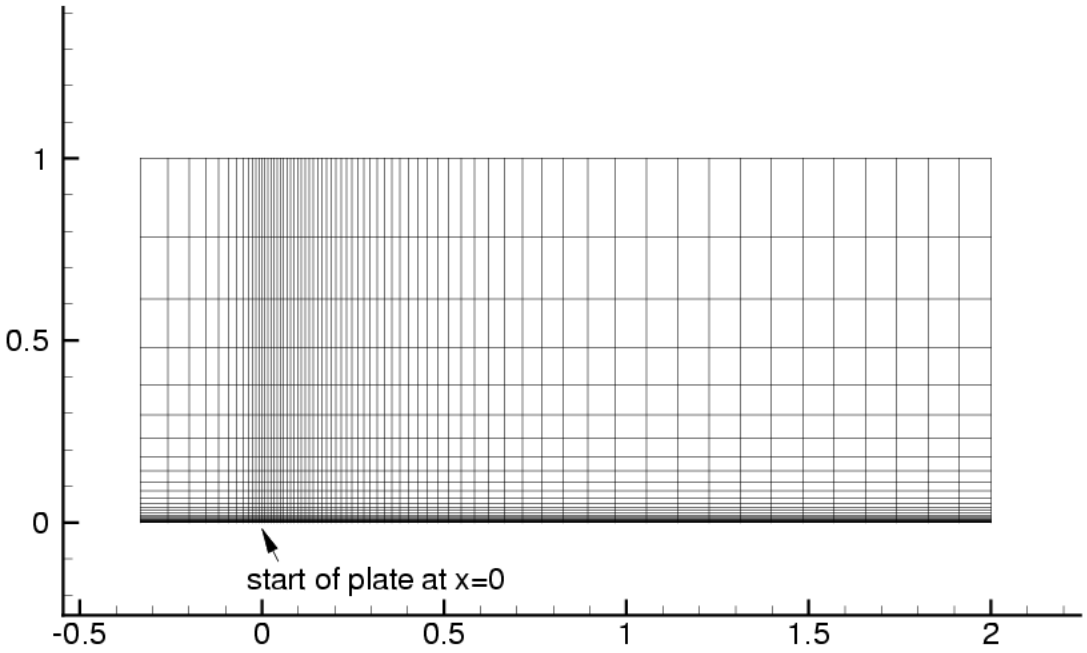

Figure 5. Flat plate grid with every fourth grid point removed in each coordinate direction for clarity.

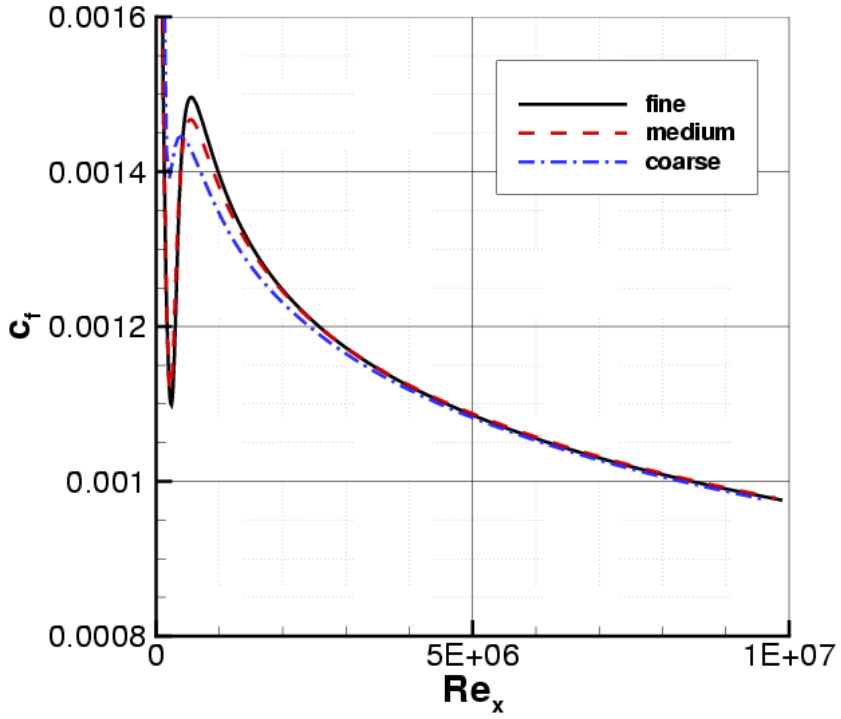

Figure 6. Wall skin friction coefficient grid study for $M = 5$, adiabatic wall, using SST on 3 successive grid sizes.

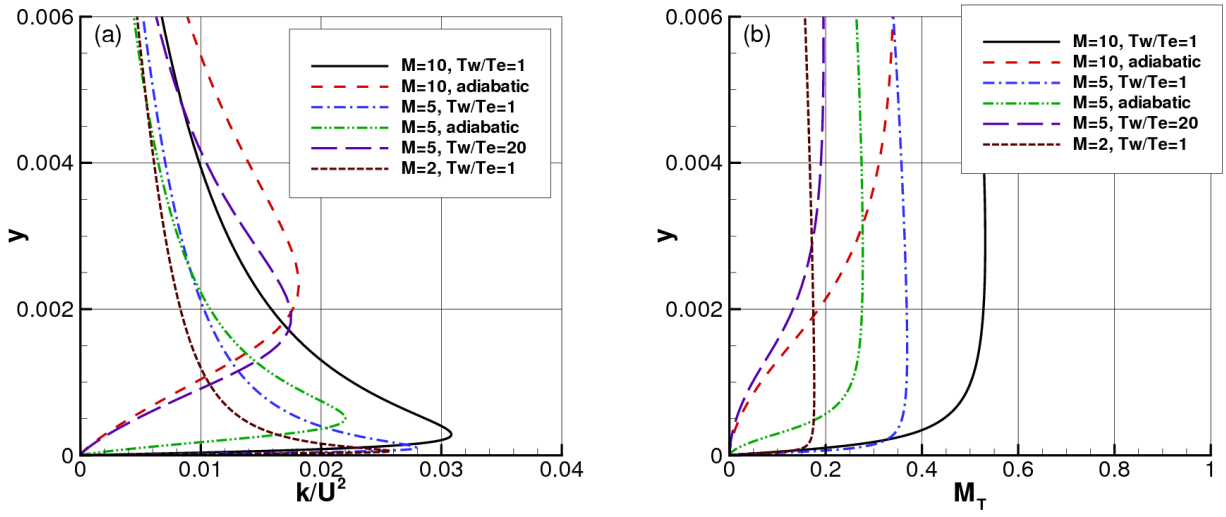

Figure 7. Profiles of local turbulent quantities in the boundary layer at $Re_x = 5 \times 10^6$, SST model: (a) k/U^2, (b) $M_T = (\sqrt{2k})/a$.

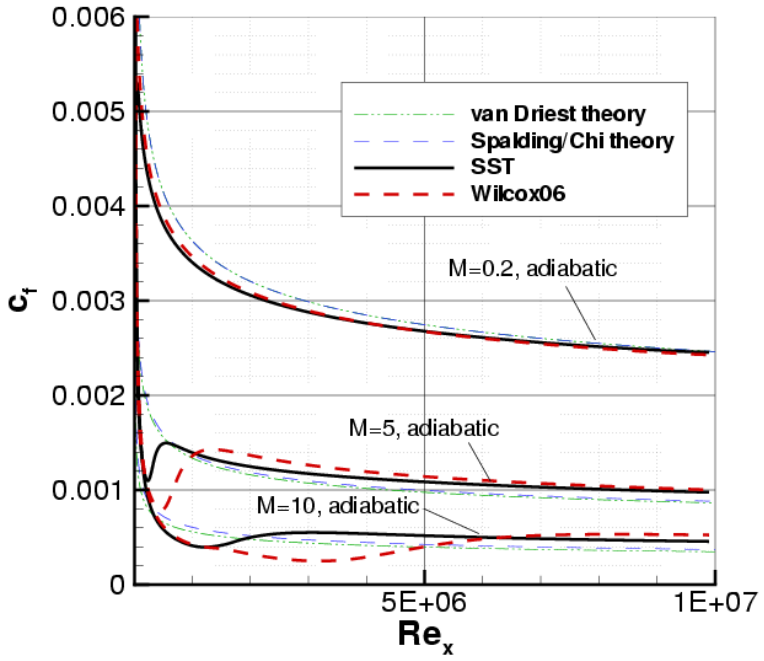

Figure 8. Wall skin friction coefficients for adiabatic wall cases.

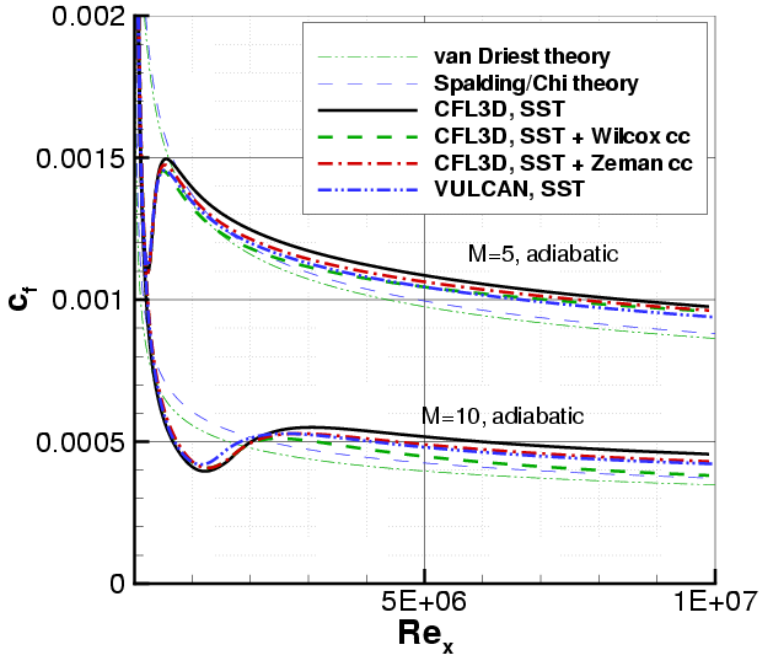

Figure 9. Effect of code and Wilcox/Zeman compressibility corrections on wall skin friction coefficients for adiabatic wall cases.

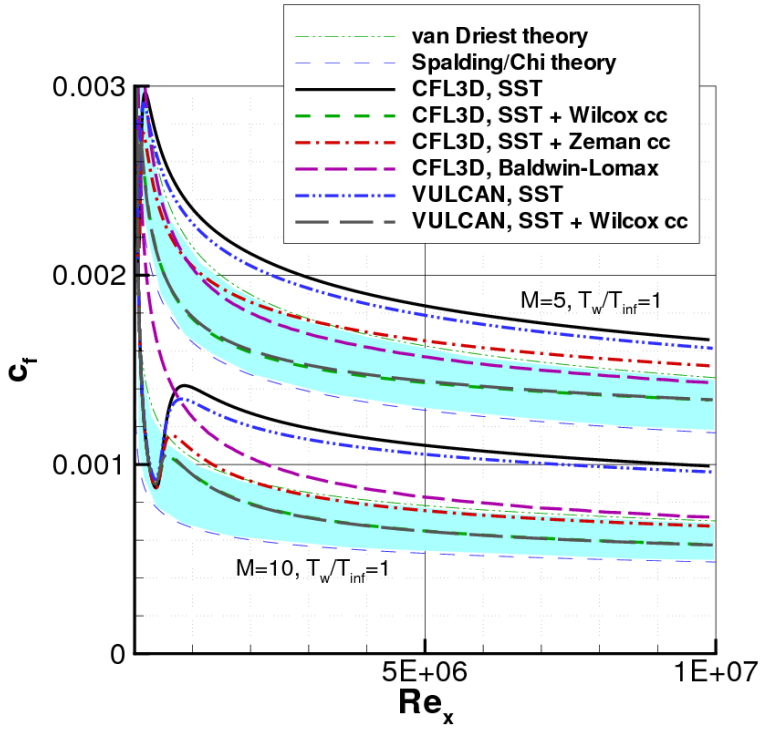

Figure 10. Wall skin friction coefficients for two cold-wall wall cases.

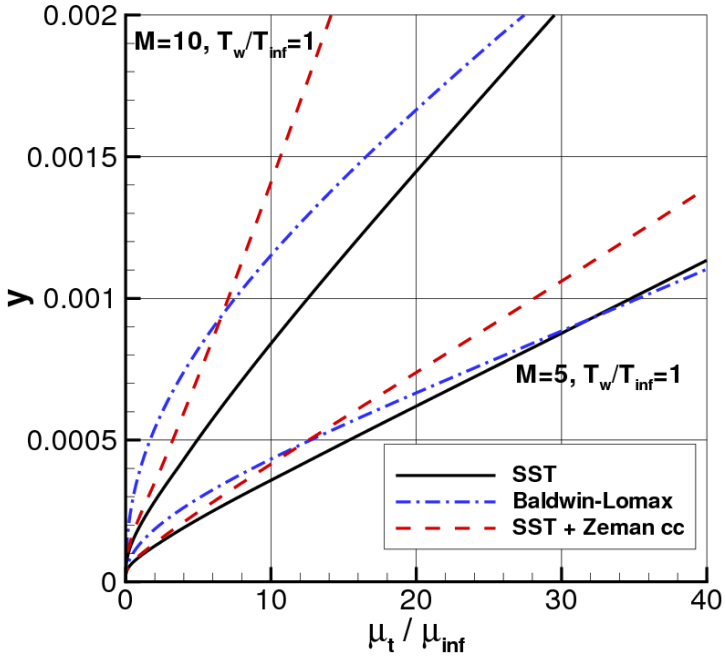

Figure 11. Profiles of nondimensional μ_t for $M = 5$ and $M = 10$ cases, $T_w/T_\infty = 1$, at $Re_x = 5 \times 10^6$.

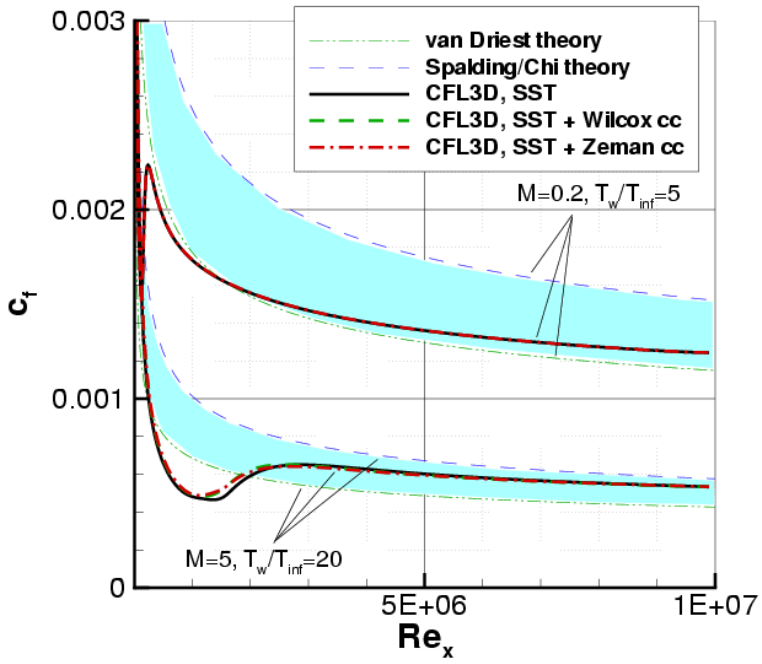

Figure 12. Wall skin friction coefficients for two hot-wall wall cases.

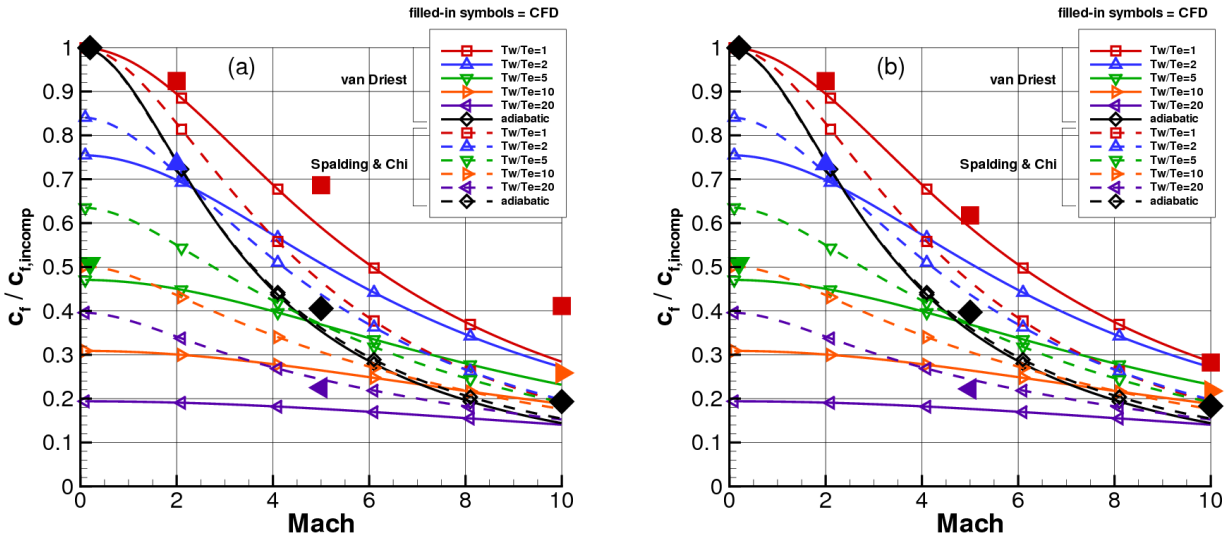

Figure 13. Theoretical compressible wall skin friction compared to incompressible level as a function of Mach number for $Re_x = 5 \times 10^6$, $T_e = 540$ R, including (a) SST (no compressibility correction), and (b) SST (Zeman compressibility correction).

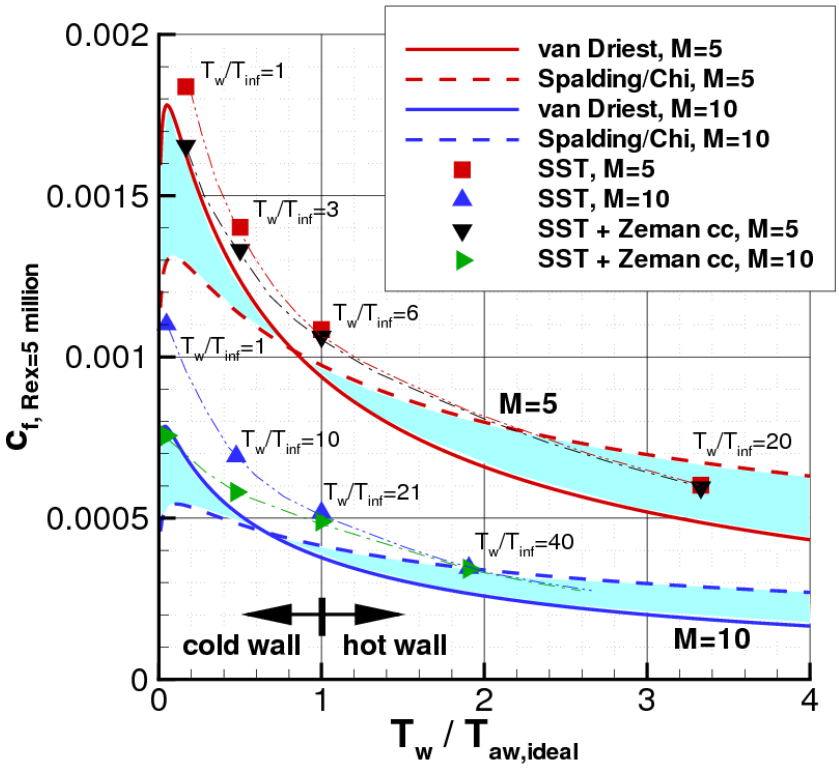

Figure 14. Compressible wall skin friction as a function of $T_w/T_{aw,ideal}$ for $Re_x = 5 \times 10^6$, $T_e = 540$ R, with SST results included.

REPORT DOCUMENTATION PAGE	Form Approved OMB No. 0704–0188

1. REPORT DATE *(DD-MM-YYYY)*	2. REPORT TYPE	3. DATES COVERED *(From - To)*
01-04-2009	Technical Memorandum	

4. TITLE AND SUBTITLE

Compressibility Considerations for k-ω Turbulence Models in Hypersonic Boundary Layer Applications

5a. CONTRACT NUMBER

5b. GRANT NUMBER

5c. PROGRAM ELEMENT NUMBER

6. AUTHOR(S)

C. L. Rumsey

5d. PROJECT NUMBER

5e. TASK NUMBER

5f. WORK UNIT NUMBER

644423.02.39.04.10.03

7. PERFORMING ORGANIZATION NAME(S) AND ADDRESS(ES)

NASA Langley Research Center
Hampton, Virginia 23681-2199

8. PERFORMING ORGANIZATION REPORT NUMBER

L–19589

9. SPONSORING/MONITORING AGENCY NAME(S) AND ADDRESS(ES)

National Aeronautics and Space Administration
Washington, DC 20546-0001

10. SPONSOR/MONITOR'S ACRONYM(S)

NASA

11. SPONSOR/MONITOR'S REPORT NUMBER(S)

NASA/TM–2009–215705

12. DISTRIBUTION/AVAILABILITY STATEMENT

Unclassified-Unlimited
Subject Category 01
Availability: NASA CASI (443) 757-5802

13. SUPPLEMENTARY NOTES

An electronic version can be found at http://ntrs.nasa.gov.

14. ABSTRACT

The ability of k-ω models to predict compressible turbulent skin friction in hypersonic boundary layers is investigated. Although uncorrected two-equation models can agree well with correlations for hot-wall cases, they tend to perform progressively worse - particularly for cold walls - as the Mach number is increased in the hypersonic regime. Simple algebraic models such as Baldwin-Lomax perform better compared to experiments and correlations in these circumstances. Many of the compressibility corrections described in the literature are summarized here. These include corrections that have only a small influence for k-ω models, or that apply only in specific circumstances. The most widely-used general corrections were designed for use with jet or mixing-layer free shear flows. A less well-known dilatation-dissipation correction intended for boundary layer flows is also tested, and is shown to agree reasonably well with the Baldwin-Lomax model at cold-wall conditions. It exhibits a less dramatic influence than the free shear type of correction. There is clearly a need for improved understanding and better overall physical modeling for turbulence models applied to hypersonic boundary layer flows.

15. SUBJECT TERMS

CFD, hypersonic, turbulence model, compressibility, skin friction

16. SECURITY CLASSIFICATION OF:			17. LIMITATION OF ABSTRACT	18. NUMBER OF PAGES	19a. NAME OF RESPONSIBLE PERSON
a. REPORT	b. ABSTRACT	c. THIS PAGE			STI Help Desk (email: help@sti.nasa.gov)
U	U	U	UU	34	19b. TELEPHONE NUMBER *(Include area code)* (443) 757-5802